Mesoporous Salts

DOI: 10.1002/anie.201107812

A Topotactic Synthetic Methodology for Highly Fluorine-Doped Mesoporous Metal Oxides**

*Zhen-an Qiao, Suree S. Brown, Jamie Adcock, Gabriel M. Veith, J. Chris Bauer, E. Andrew Payzant, Raymond R. Unocic, and Sheng Dai**

Ordered mesoporous materials have attracted much attention for years because of their excellent physical properties, such as very large specific surface area, nanometer-scale fine pores, and high stability,[1] which are beneficial for their use as catalysts,[2] separators,[3] adsorbents,[4] and so forth. The first ordered mesoporous materials were synthesized in around 1990 using soft templating pathways.[5] Following the soft templating method, different kinds of mesoporous silica[6] and nonsilica materials such as carbon,[7] metal phosphates,[8] γ-Al_2O_3,[9] Cr_2O_3,[10] lanthanide oxides,[11] TiO_2, ZrO_2, Al_2O_3, Nb_2O_5, Ta_2O_5, and WO_3 were synthesized.[12] Nanocasting is an alternative method for preparing mesoporous materials that are difficult to synthesize with the conventional soft templating method.[13] This hard templating approach has been applied to prepare different kinds of metal oxides, such as CoO,[14] Co_3O_4,[15] Mn_3O_4,[16] Fe_2O_3,[17] Fe_3O_4,[18] and NiO.[19] Following the work by Lu et al.,[20] several ordered mesoporous materials, including MgO,[21] boron nitride,[22] γ-Al_2O_3,[23] aluminosilicate,[24] CuO,[25] and ZnO,[26] were nanocast by using ordered mesoporous carbon CMK-3 as a matrix.

The control of interfacial properties through tunable surface functionalities is essential in the development of functional mesoporous materials. To the best of our knowledge, no versatile method for preparation of fluorine-doped mesoporous metal oxides has been reported previously. Mesoporous materials with high F atomic concentrations could be considered as a new class of mesoporous materials (mesoporous metal oxyfluorides). Owing to the high acidity of host frameworks, favorable fluoride ionic conduction and a spectral response in the visible region, these materials have properties of interest for numerous potentially valuable applications such as electric conductors, primary and secondary batteries, catalysis, and photocatalysis.[27] There are only three reports on fluorine-containing mesoporous materials for mesoporous carbons prepared in a one-pot synthesis route using *p*-fluorophenol/phenol–formaldehyde as carbon precursors or through direct fluorination.[28]

By employing mesoporous metal oxides (TiO_2 ZrO_2, Al_2O_3, Nb_2O_5, and Ta_2O_5) as the starting materials and by using the most reactive fluorination agent, elemental fluorine (F_2), we developed a novel, straightforward topotactic route towards F-doped mesoporous metal oxides with high fluorine content (up to 40%). The BET surface areas, pore sizes, pore volumes, and F atomic concentrations for these materials could be adjusted by varying the fluorination time and temperature (BET = Brunauer–Emmett–Teller). Our topotactic preparation method presents a general and facile approach to synthesis of F-doped mesoporous metal oxides and could be carried out on a large scale.

Mesoporous metal oxides can be synthesized easily by a solvent-evaporation-induced self-assembly method by using metal alkoxides as the metal source and triblock copolymer F127 as the template.[12b] The overall synthetic procedure is illustrated in Scheme 1. We used five typical mesoporous metal oxides as precursors: TiO_2, ZrO_2, Al_2O_3, Nb_2O_5, and Ta_2O_5. The topotactic reaction proceeded by the chemical substitution of O atoms in the metal oxides by F atoms, resulting in F-doped mesoporous metal oxides. In other words, these mesoporous materials with crystalline (TiO_2) or

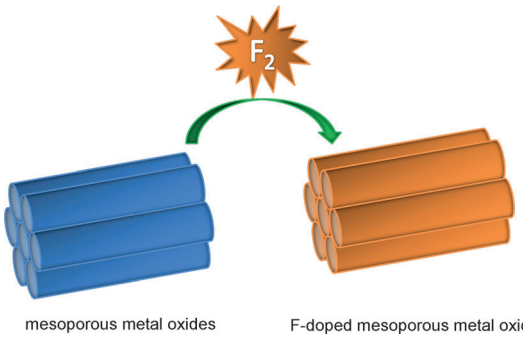

Scheme 1. Preparation procedure of fluorine-doped mesoporous metal oxides.

[*] Dr. Z. A. Qiao, Dr. S. S. Brown, Dr. J. Adcock, Dr. S. Dai
Department of Chemistry, University of Tennessee
Knoxville, TN 37996 (USA)
E-mail: dais@ornl.gov
Dr. J. C. Bauer, Dr. S. Dai
Chemical Sciences Division, Oak Ridge National Laboratory
Oak Ridge, TN 37831 (USA)
Dr. E. A. Payzant
Center for Nanophase Material Sciences, Oak Ridge National Laboratory (USA)
Dr. G. M. Veith, Dr. R. R. Unocic
Materials Science and Technology Division, Oak Ridge National Laboratory (USA)

[**] This work was sponsored by the Materials Sciences and Engineering Division (Z.A.Q., J.A., G.M.V., R.R.U., S.D.) and the Division of Chemical Sciences, Geosciences, and Biosciences (S.B., J.C.B.), Office of Basic Energy Sciences, US Department of Energy. A portion of this research was conducted at the Center for Nanophase Materials Sciences, which is sponsored at Oak Ridge National Laboratory by the Office of Basic Energy Sciences, US Department of Energy. Microscopy was supported by ORNL's Shared Research Equipment (SHaRE) User Facility, which is sponsored by the Office of Basic Energy Sciences, US Department of Energy.

Supporting information for this article is available on the WWW under http://dx.doi.org/10.1002/anie.201107812.

amorphous structure (ZrO_2, Al_2O_3, Nb_2O_5, and Ta_2O_5) were fluorinated into F-doped mesoporous metal oxides by treatment with F_2 gas.

We take mesoporous TiO_2 as a representative sample to describe the preparation method. Mesoporous TiO_2 was dried at 150 °C under vacuum (< 10 mTorr) overnight prior to fluorination. Dehydrated mesoporous TiO_2 (ca. 0.5 g) was placed in a fluidized bed fluorination reactor (FBR). The FBR tube was purged for 1.5 h with 46 sccm helium (sccm = standard cubic centimeters per minute), while the temperature at the bottom of the FBR tube was ramped to the set temperature. After 30 min, fluorine at 3.2 sccm was introduced into the reactor along with the helium flow (F_2/He = 7 vol %). After the allotted reaction time, the FBR tube was purged with helium, cooled to room temperature, unsealed, and weighed. Finally, a bright yellow colored powder of the F-doped mesoporous TiO_2 was obtained. Because one O atom was substituted by two F atoms during the reaction, the weight increased from 0.5 g to 0.554 g for the TiO_2 fluorinated at 75 °C for 2 days.

The crystal phase and the composition of the F-doped mesoporous TiO_2 were determined by wide-angle X-ray diffraction (WXRD) analysis. The WXRD patterns of pristine mesoporous TiO_2 and the fluorinated mesoporous TiO_2 show the evolution of the crystal phases (Figure 1). The

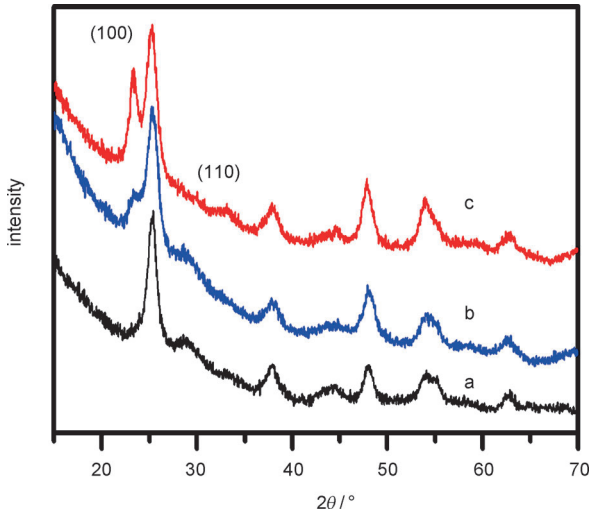

Figure 1. XRD patterns for pristine mesoporous TiO_2 (a), F-doped mesoporous TiO_2 fluorinated at room temperature for 2 days (b), and 75 °C for 2 days (c).

pristine mesoporous TiO_2 shows well-crystallized anatase peaks without any impurity phase. After TiO_2 was fluorinated at room temperature (22–24 °C) for 2 days, the WXRD pattern showed a new diffraction peak at $2\theta = 23.4°$, corresponding to the (100) plane diffraction of the cubic $TiOF_2$ phase and suggesting the formation of $TiOF_2$ nanocrystallites. Increasing the fluorination temperature up to 75 °C greatly enhances the diffraction intensities of cubic $TiOF_2$, indicating that the crystallinity and the particle size increase. Simultaneously, another new diffraction peak at $2\theta = 33.1°$ appears, corresponding to the (110) plane diffraction of $TiOF_2$. The average size of the $TiOF_2$ nanocrystals was calculated from Scherrer's formula to be 9.5 nm. However, TiO_2 structures fluorinated at room temperature or 75 °C for 1 day did not have obvious change, which indicates that F atoms just substitute for the O atoms in the framework of mesoporous TiO_2 for these samples. Thus, by adjusting the reaction time and temperature, we could obtain both F-doped mesoporous TiO_2 and mesoporous TiO_2–$TiOF_2$ nanocomposites. It is worth mentioning that reaction temperatures for the fluorination of TiO_2 should not exceed 150 °C. Otherwise, substantial sublimation and loss of TiF_4, with the flowing He, could occur.

N_2 adsorption–desorption isotherms and pore size distribution curves of F-doped mesoporous TiO_2 composites with different fluorination times and temperatures are shown in Figure 2 a, and the corresponding pore properties, including BET surface areas, pore volumes, and pore sizes, are summarized in Table 1. The isotherms of F-doped mesoporous TiO_2 with various fluorination times at room temper-

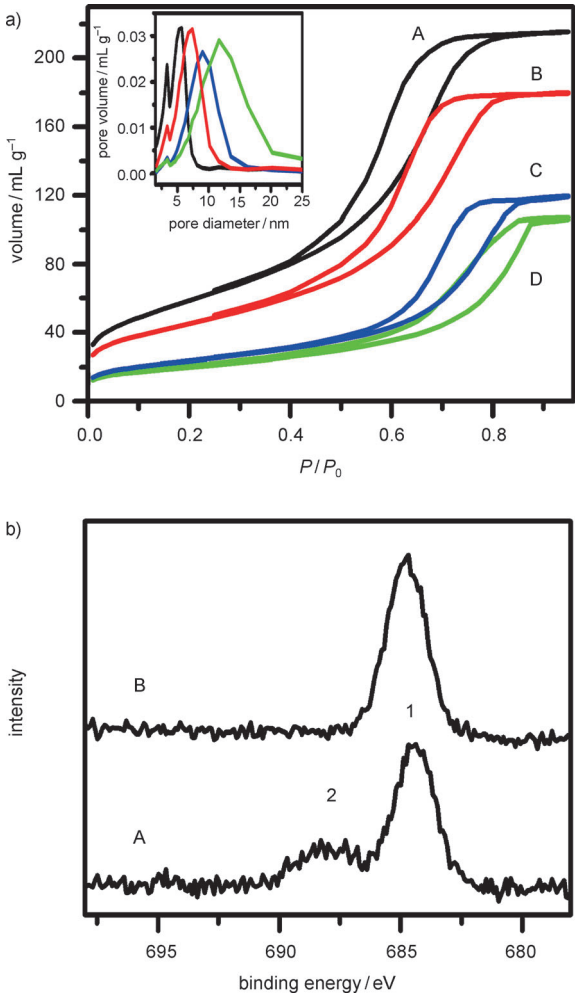

Figure 2. a) Nitrogen adsorption–desorption isotherms for pristine mesoporous TiO_2 (A), F-doped mesoporous TiO_2 fluorinated at room temperature for 18 h (B), room temperature for 2 days (C), and 75 °C for 2 days (D). The inset shows the corresponding pore size distribution. b) F 1s XPS spectra for F-doped mesoporous TiO_2 fluorinated at room temperature (A) and 75 °C (B) for 2 days.

Table 1: Structural properties of F-doped mesoporous TiO_2 prepared under various fluorination conditions.

T [°C][a]	*t* [h][b]	BET [$m^2 g^{-1}$][c]	*V* [$cm^3 g^{-1}$][d]	*S* [nm][e]
RT[f]	4	214	0.331	6.1
RT	18	163	0.277	7.3
RT	48	84	0.181	9.0
75	24	143	0.227	7.9
75	48	71	0.160	12.0

[a] Fluorination temperature; [b] fluorination time; [c] BET surface area; [d] pore volume; [e] pore size; [f] room temperature (22–24 °C).

ature exhibit characteristic type IV curves with distinct capillary condensation steps, suggesting uniform mesopores, and the pore geometry does not change after fluorination. The pore sizes calculated from the adsorption data using the BJH (Barrett–Joyner–Halenda) model are in a wide range of 5.7–9.0 nm, increasing with an increase in fluorination time. The BET specific surface areas are as high as 84–245 $m^2 g^{-1}$, decreasing with an increase in fluorination time. After being fluorinated at 75 °C in F_2 gas for 2 days, the mesoporous TiO_2–$TiOF_2$ nanocomposites show a capillary condensation step with a slightly wide relative pressure range of 0.57–0.83, suggesting a wide mesopore size distribution. The calculated mean size is as large as 12.0 nm, which is much larger than that of the pristine mesoporous TiO_2 (5.7 nm). The BET surface area and pore volume are about 71 $m^2 g^{-1}$ and 0.160 $cm^3 g^{-1}$, respectively, clearly indicating an enlarged mesopore by F_2 gas etching and an increased wall density from fluorination. Transmission electron microscopy (TEM) images (Figure S1 in the Supporting Information) and small-angle X-ray diffraction (SAXRD) patterns (Figure S2) for these samples further confirm that pore sizes increased and the general pore morphologies become less ordered with fluorination time and temperature. Additionally, EDX elemental images (Figure S3) show that the distribution of fluorine within the TiO_2 structure is very homogeneous.

The surface composition and the corresponding binding energy values of the respective elements (Ti, O, and F) present in the F-doped mesoporous TiO_2 were analyzed by X-ray photoelectron spectroscopy (XPS). The peaks observed at 684.8 and 688.6 eV for F 1s (Figure 2b), 459 and 465 eV for Ti $2p_{3/2}$ and Ti $2p_{1/2}$, 530.3 eV for O 1s (Figure S4), and their corresponding intensities were used to determine quantitatively the concentration of the species present in the samples. A nearly symmetrical F1s peak at 684.8 eV was observed for mesoporous TiO_2–$TiOF_2$ fluorinated at 75 °C for 2 days, which contains a pure $TiOF_2$ phase. However, a new peak appeared for the sample prepared at room temperature for 2 days, indicating that the F atoms in this F-doped mesoporous TiO_2 have two different chemical forms. In agreement with previously reports,[29] the peak (1) located at 684.8 eV originated from the F atoms of the $TiOF_2$. The second F peak (2) located at 688.6 eV is attributed to the doped F atoms in TiO_2, that is, the substitutional F atoms that occupy oxygen sites in the TiO_2 crystal lattice. These results indicate that some of the F atoms in this sample exist in the form of $TiOF_2$ while others are doped F atoms in $TiO_{2-x}F_x$. This result indicates that F atoms are physically adsorbed on the surface of TiO_2 and replace the O atoms in the crystal lattice at the beginning of the reaction. When the concentration of F atom exceeds a specific value as fluorination temperature and time increase, F-doped mesoporous TiO_2 further crystallizes to mesoporous TiO_2–$TiOF_2$. Accordingly, the calculated Ti/O/F atomic ratio of mesoporous TiO_2–$TiOF_2$ fluorinated at 75 °C is 24.0:54.3:21.7, and that of TiO_2 to $TiOF_2$ species in the framework of the sample is approximately 2.5:1.

At the specified calcination temperature (350 °C), the wall structures of mesoporous Nb_2O_5, Al_2O_3, ZrO_2, and Ta_2O_5 are amorphous, which is easier to be substituted and etched by treatment with F_2 gas than the mesoporous anatase TiO_2 with crystallized structures. Additionally, because of the low sublimation temperatures of NbF_5 (120 °C under vacuum) and TaF_5 (room temperature under vacuum), only room temperature was used for fluorination of these amorphous metal oxides. The fluorination time for these mesoporous metal oxides was shorter, and much smaller excesses of fluorine were used as relative to those for TiO_2. For these mesoporous metal oxides, whether increasing fluorination temperature or extending fluorination time, we could not observe a new diffraction peak in their WXRD patterns, suggesting that these samples maintained their amorphous structure after being fluorinated.

The BET surface areas for the fluorinated mesoporous Nb_2O_5, Al_2O_3, ZrO_2, and Ta_2O_5 have a similar declining trend with that for F-doped mesoporous TiO_2. Increasing the reaction time for these mesoporous materials had a dramatic effect upon their BET surface areas, decreasing from 167 to 53 $m^2 g^{-1}$ for Nb_2O_5, from 228 to 115 $m^2 g^{-1}$ for Al_2O_3, 86 to 24 $m^2 g^{-1}$ for ZrO_2, and 52 to 15 $m^2 g^{-1}$ for Ta_2O_5 (Figure 3, Figure S5 and Table S1). Additionally, pore sizes increased steadily, from 6.1 to 9.8 nm for Nb_2O_5, 4.3 to 7.2 nm for Al_2O_3, 3.5 to 5.5 nm for ZrO_2, and 4.7 to 5.2 nm for Ta_2O_5. After fluorination of mesoporous Ta_2O_5 for 18 h, the BET surface area decreased greatly, while the pore size did not change significantly (Figure S5). This observation with the increase in fluorination time is consistent with the greatly increased F content in the wall of the mesostructure of Ta_2O_5. In combination with the BET results for F-doped mesoporous TiO_2, we can conclude that BET surface areas, pore sizes, and pore volumes for the F-doped mesoporous materials could be controlled in a wide range by adjusting the fluorination time and temperature.

Figure 3d shows the high-resolution F1s XPS spectra of F-doped mesoporous ZrO_2 fluorinated at room temperature for 2 days. The F 1s peak (685.7 eV) determined for this sample is consistent with the formation of F-doped ZrO_2 species. The O1s peak was centered at 530.2 eV, which is consistent with Zr–O moieties trapped in the sample. The calculated Zr/O/F atomic ratio of the F-doped mesoporous ZrO_2 is 22.2:36.6:41.2; therefore, the ZrO_2 to F-doped ZrO_2 species in the framework of the sample is approximately 2:1. The XPS spectra for the Zr 3d contains two different Zr species (Figure S6). Deconvoluting the peak structure reveals the formation of two overlapping Zr species; Zr–O (Zr $3d_{5/2}$ = 183 eV, Zr $3d_{3/2}$ = 185.8) and Zr–F (Zr $3d_{5/2}$ = 184.8 eV, Zr $3d_{3/2}$ = 187.3 eV). The binding energies of the Zr–O and Zr–F are

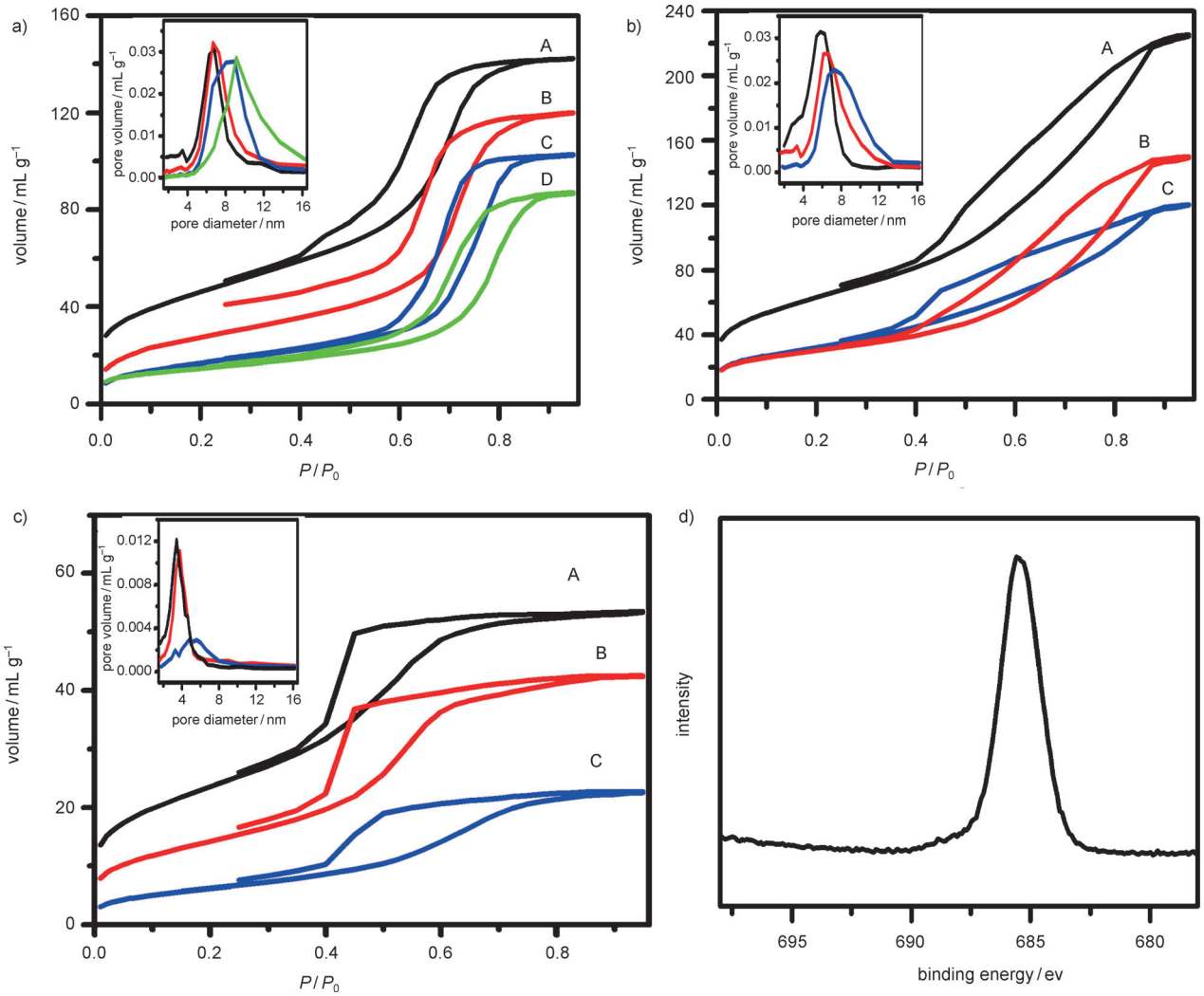

Figure 3. a) Nitrogen adsorption–desorption isotherms for pristine mesoporous Nb_2O_5 (A), F-doped mesoporous Nb_2O_5 fluorinated at room temperature for 4 h (B), 18 h (C), and 2 days (D). b) Nitrogen adsorption–desorption isotherms for pristine mesoporous Al_2O_3 (A), F-doped mesoporous Al_2O_3 fluorinated at room temperature for 18 h (B), and 2 days (C). c) Nitrogen adsorption–desorption isotherms for pristine mesoporous ZrO_2 (A), F-doped mesoporous ZrO_2 fluorinated at room temperature for 18 h (B), and 2 days (C). The insets show the corresponding pore size distributions. d) F 1s XPS spectra for F-doped mesoporous ZrO_2 fluorinated at room temperature for 2 days.

consistent with those reported previously.[30] The other amorphous F-doped mesoporous materials have similar XPS results. Accordingly, the calculated metal/O/F atomic ratios of the Nb_2O_5, Al_2O_3, and Ta_2O_5 fluorinated for 18 h are 22:57.3:20.7, 20.9:38.8:40.3, and 21.5:46.1:32.4, respectively, which corroborate with the nominal atomic composition. Therefore, although only room temperature is used for fluorinations of these amorphous mesoporous metal oxides, the calculated F atomic concentrations in these samples are as high as 20.7–40.3 at %. Additionally, the reactivity with F_2 gas is on the order of $Al_2O_3 > Ta_2O_5 > ZrO_2 > Nb_2O_5 > TiO_2$.

Thermogravimetric analysis (TGA) in N_2 was performed on the F-doped mesoporous metal oxides to investigate their thermal stability and calculate the weight percentages of F atoms in these samples. Figure 4 illustrates a weight loss of 8–20 wt % between 100 and 800 °C for all the samples. The F-doped mesoporous TiO_2 exhibits a weight loss at 100–400 °C, which can be attributed primarily to desorption of F atoms on

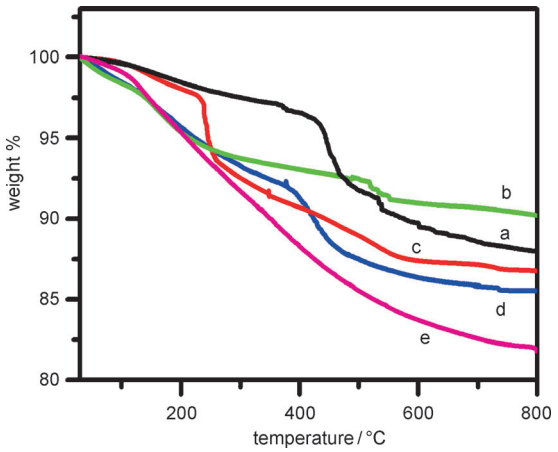

Figure 4. TGA curves for F-doped mesoporous TiO_2 fluorinated at 75 °C for 2 days (a), Nb_2O_5 (b), ZrO_2 (c), Ta_2O_5 (d), and Al_2O_3 (e) fluorinated at room temperature for 18 h.

the surface of mesoporous materials. Another key weight loss occurring at 400–600 °C could be ascribed to the decomposition of remaining F in the framework of mesoporous materials and to phase transformation from $TiOF_2$ to anatase. The F-doped Nb_2O_5 and Ta_2O_5 have TGA results similar to those with TiO_2. F-doped Al_2O_3 shows much gentler weight loss at temperatures of 100–800 °C, indicating that the distribution of F atoms in the Al_2O_3 framework is very homogeneous. However, the fast weight loss for F-doped ZrO_2 occurred at temperatures of 200–250 °C, which indicates that the F-doped ZrO_2 is much less stable than the F-doped TiO_2. The TGA results further confirm the high F atomic concentrations in these fluorinated mesoporous materials.

In summary, a general topotactic synthesis strategy to prepare F-doped mesoporous metal oxides was demonstrated by using mesoporous metal oxides as starting materials and fluorine as the fluorination agent. This approach is versatile and takes advantage of porous nature of mesoporous oxides, leading to a facile incorporation of fluoride ions into lattices without change of mesoporous structures. The resultant fluorine constituent distributions and pore structure of the final F-doped mesoporous products are highly controllable by adjusting the reaction conditions. The calculated F atomic concentrations in these materials are as high as 20.7–40.3 %. This topotactic synthesis strategy can also be extended to synthesize F-doped other mesoporous metal oxides, mesoporous mixed-metal oxides, mesoporous metal phosphates, zeolites, and oxide nanostructures.

Experimental Section

Synthesis of mesoporous metal oxides: Mesoporous metal oxides were prepared as described earlier.[12b] In a typical synthesis of mesoporous TiO_2, $Ti(OBu)_4$ (10 mmol), HOAc (40 mmol), HCl (24 mmol), and F127 ($EO_{96}PO_{70}EO_{96}$, MW = 12000 g mol^{-1}, 1.6 g) were dissolved in 30 mL of ethanol. The mixture was stirred vigorously for 1 h and transferred into a petri dish. The ethanol was evaporated at 40 °C. A transparent membrane was formed after 12 h, and it was transferred into a 65 °C oven and aged for an additional 24 h. As-synthesized mesostructured hybrids were calcined at 350 °C in air for 5 h (ramp rate 2 °C min^{-1}) to obtain mesoporous TiO_2.

Fluorinations of mesoporous metal oxides: Mesoporous metal oxides, TiO_2, ZrO_2, Nb_2O_5, Ta_2O_5, and Al_2O_3 were dried at 150 °C under vacuum (< 10 mTorr) overnight prior to fluorination. All fluorinations were conducted in a fluidized bed fluorination reactor (FBR). The reactor was connected to a mixing device consisting of a Hastings flow transducer calibrated for fluorine and a rotameter gauge flowmeter for helium gas. The apparatus allowed for He/F_2 mixtures from 0 to 100 % fluorine to flow into the FBR tube. Dehydrated mesoporous TiO_2, ZrO_2, Nb_2O_5, Ta_2O_5, or Al_2O_3 (ca. 0.5 g) was placed in an FBR tube sealed using teflon tape on the sealing surfaces and weighed. The FBR tube was purged for 90 min with 46 sccm helium while the temperature at the bottom of the FBR tube was ramped to the set temperature. After 30 min, fluorine at 3.2 sccm (for TiO_2) or 0.8 sccm (for ZrO_2, Nb_2O_5, Ta_2O_5, and Al_2O_3) was introduced into the reactor along with the helium flow at $F_2/He = 7$ vol % (for TiO_2) or $F_2/He = 5$ vol % for ZrO_2, Nb_2O_5, Ta_2O_5, and Al_2O_3). After the allotted reaction time, the FBR tube was purged with helium (46 sccm), sealed, and weighed.

Characterization: X-ray diffraction patterns were obtained on a PANalytical Empyrean diffractometer using $Cu_{K\alpha}$ radiation. The adsorption–desorption isotherms of nitrogen were measured at −196 °C using a Micrometeritics Gemini system. The pore size distributions were calculated from the adsorption branches of N_2 adsorption–desorption isotherms based on the BJH model. The thermogravimetric curve was recorded with a TGA/DTA 320 series of TA instrument with a heating rate of 10 °C min^{-1}. XPS data were collected with a PHI 3056 XPS spectrometer with an Al source. Transmission electron microscopy (TEM) and high-resolution TEM (HRTEM) images were acquired on a FEI Titan microscope (300 kV). EDX spectra were acquired using a Phillips CM200 TEM instrument (200 kV).

Received: November 6, 2011
Revised: December 9, 2011
Published online: February 6, 2012

Keywords: doping · fluorine · mesoporous materials · synthetic methods

[1] a) Y. Wan, D. Y. Zhao, *Chem. Rev.* **2007**, *107*, 2821; b) F. Schüth, *Chem. Mater.* **2001**, *13*, 3184.
[2] A. Corma, *Chem. Rev.* **1997**, *97*, 2373.
[3] M. J. MacLachlan, N. Coombs, G. A. Ozin, *Nature* **1999**, *397*, 681.
[4] a) Z. X. Wu, D. Y. Zhao, *Chem. Commun.* **2011**, *47*, 3332; b) M. Kruk, M. Jaroniec, *Chem. Mater.* **2001**, *13*, 3169.
[5] a) J. S. Beck, J. C. Vartuli, W. J. Roth, M. E. Leonowicz, C. T. Kresge, K. D. Schmitt, C. T. W. Chu, D. H. Olson, E. W. Sheppard, S. B. McCullen, J. B. Higgins, J. L. Schlenker, *J. Am. Chem. Soc.* **1992**, *114*, 10834; b) T. Yanagisawa, T. Shimizu, K. Kuroda, C. Kato, *Bull. Chem. Soc. Jpn.* **1990**, *63*, 988.
[6] D. Y. Zhao, J. L. Feng, Q. S. Huo, N. Melosh, G. H. Fredrickson, B. F. Chmelka, G. D. Stucky, *Science* **1998**, *279*, 548.
[7] Y. Wan, H. F. Yang, D. Y. Zhao, *Acc. Chem. Res.* **2006**, *39*, 423.
[8] B. Z. Tian, X. Y. Liu, B. Tu, C. Z. Yu, J. Fan, L. M. Wang, S. H. Xie, G. D. Stucky, D. Y. Zhao, *Nat. Mater.* **2003**, *2*, 159.
[9] a) Z. R. Zhang, R. W. Hicks, T. R. Pauly, T. J. Pinnavaia, *J. Am. Chem. Soc.* **2002**, *124*, 1592; b) M. Kuemmel, D. Grosso, U. Boissiere, B. Smarsly, T. Brezesinski, P. A. Albouy, H. Amenitsch, C. Sanchez, *Angew. Chem.* **2005**, *117*, 4665; *Angew. Chem. Int. Ed.* **2005**, *44*, 4589.
[10] A. K. Sinha, K. Suzuki, *Angew. Chem.* **2005**, *117*, 275; *Angew. Chem. Int. Ed.* **2005**, *44*, 271.
[11] D. M. Lyons, L. P. Harman, M. A. Morris, *J. Mater. Chem.* **2004**, *14*, 1976.
[12] a) P. D. Yang, D. Y. Zhao, D. I. Margolese, B. F. Chmelka, G. D. Stucky, *Nature* **1998**, *396*, 152; b) J. Fan, S. W. Boettcher, G. D. Stucky, *Chem. Mater.* **2006**, *18*, 6391; c) S. W. Boettcher, J. Fan, C. K. Tsung, Q. H. Shi, G. D. Stucky, *Acc. Chem. Res.* **2007**, *40*, 784.
[13] a) R. Ryoo, S. H. Joo, S. Jun, *J. Phys. Chem. B* **1999**, *103*, 7743; b) Y. F. Shi, Y. Wan, D. Y. Zhao, *Chem. Soc. Rev.* **2011**, *40*, 3854.
[14] H. Tüysüz, Y. Liu, C. Weidenthaler, F. Schüth, *J. Am. Chem. Soc.* **2008**, *130*, 14108.
[15] a) B. Z. Tian, X. Y. Liu, L. A. Solovyov, Z. Liu, H. F. Yang, Z. D. Zhang, S. H. Xie, F. Q. Zhang, B. Tu, C. Z. Yu, O. Terasaki, D. Y. Zhao, *J. Am. Chem. Soc.* **2004**, *126*, 865; b) Y. Q. Wang, C. M. Yang, W. Schmidt, B. Spliethoff, E. Bill, F. Schuth, *Adv. Mater.* **2005**, *17*, 53.
[16] F. Jiao, A. Harrison, A. H. Hill, P. G. Bruce, *Adv. Mater.* **2007**, *19*, 4063.
[17] F. Jiao, A. Harrison, J. C. Jumas, A. V. Chadwick, W. Kockelmann, P. G. Bruce, *J. Am. Chem. Soc.* **2006**, *128*, 5468.
[18] F. Jiao, J. C. Jumas, M. Womes, A. V. Chadwick, A. Harrison, P. G. Bruce, *J. Am. Chem. Soc.* **2006**, *128*, 12905.
[19] F. Jiao, A. H. Hill, A. Harrison, A. Berko, A. V. Chadwick, P. G. Bruce, *J. Am. Chem. Soc.* **2008**, *130*, 5262.

[20] A. H. Lu, W. Schmidt, A. Taguchi, B. Spliethoff, B. Tesche, F. Schuth, *Angew. Chem.* **2002**, *114*, 3639; *Angew. Chem. Int. Ed.* **2002**, *41*, 3489.
[21] J. Roggenbuck, M. Tiemann, *J. Am. Chem. Soc.* **2005**, *127*, 1096.
[22] P. Dibandjo, L. Bois, F. Chassagneux, D. Cornu, J. M. Letoffe, B. Toury, F. Babonneau, P. Miele, *Adv. Mater.* **2005**, *17*, 571.
[23] Q. Liu, A. Q. Wang, X. D. Wang, T. Zhang, *Chem. Mater.* **2006**, *18*, 5153.
[24] Y. M. Fang, H. Q. Hu, *J. Am. Chem. Soc.* **2006**, *128*, 10636.
[25] X. Y. Lai, X. T. Li, W. C. Geng, J. C. Tu, J. X. Li, S. L. Qiu, *Angew. Chem.* **2007**, *119*, 752; *Angew. Chem. Int. Ed.* **2007**, *46*, 738.
[26] T. Wagner, T. Waitz, J. Roggenbuck, M. Froba, C. D. Kohl, M. Tiemann, *Thin Solid Films* **2007**, *515*, 8360.
[27] a) N. Recham, J. N. Chotard, L. Dupont, C. Delacourt, W. Walker, M. Armand, J. M. Tarascon, *Nat. Mater.* **2010**, *9*, 68; b) S. Schäfer, T. Wirth, *Angew. Chem.* **2010**, *122*, 2846; *Angew. Chem. Int. Ed.* **2010**, *49*, 2786; c) S. Chaudhuri, F. Wang, C. P. Grey, *J. Am. Chem. Soc.* **2002**, *124*, 11746; d) J. Zhu, D. Q. Zhang, Z. F. Bian, G. S. Li, Y. N. Huo, Y. F. Lu, H. X. Li, *Chem. Commun.* **2009**, 5394.
[28] a) Y. Wan, X. Qian, N. Q. Jia, Z. Y. Wang, H. X. Li, D. Y. Zhao, *Chem. Mater.* **2008**, *20*, 1012; b) Z. J. Li, G. D. Del Cul, W. F. Yan, C. D. Liang, S. Dai, *J. Am. Chem. Soc.* **2004**, *126*, 12782; c) P. F. Fulvio, S. S. Brown, J. Adcock, R. T. Mayes, B. K. Guo, X. G. Sun, S. M. Mahurin, G. M. Veith, S. Dai, *Chem. Mater.* **2011**, *23*, 4420.
[29] a) J. C. Yu, J. G. Yu, W. K. Ho, Z. T. Jiang, L. Z. Zhang, *Chem. Mater.* **2002**, *14*, 3808; b) H. G. Jung, C. S. Yoon, J. Prakash, Y. K. Sun, *J. Phys. Chem. C* **2009**, *113*, 21258; c) D. Li, H. Haneda, S. Hishita, N. Ohashi, *Chem. Mater.* **2005**, *17*, 2588.
[30] a) L. P. Zhang, T. Fan, P. W. Wang, *J. Mater. Sci.* **1995**, *30*, 1445; b) A. P. Rizzato, C. V. Santilli, S. H. Pulcinelli, Y. Messaddeq, P. Hammer, *J. Sol-Gel Sci. Technol.* **2004**, *32*, 155.

